Comparison of ray-matrix and finite-difference methods in a simple 1-D velocity model

Luděk Klimeš

Department of Geophysics, Faculty of Mathematics and Physics, Charles University, Ke Karlovu 3, 121 16 Praha 2, Czech Republic (http://sw3d.cz/staff/klimes.htm)

Received: August 1, 2018; Revised: November 27, 2018; Accepted: December 11, 2018

ABSTRACT

The ray–matrix method can extend the applicability of ray methods to 3–D heterogeneous velocity models containing thin stacks of fine isotropic or anisotropic layers. Ray–matrix synthetic seismograms are compared with finite–difference synthetic seismograms in a simple 1–D velocity model, consisting of a low velocity layer covering a homogeneous halfspace. The agreement between the ray–matrix and finite–difference synthetic seismograms is very good. Moreover, the ray–matrix seismograms do not suffer from extremely thin layers, from anisotropy, and from reflections from the non–reflecting boundaries typical for finite differences.

Keywords: ray methods, matrix methods, Green function, synthetic seismograms

1. INTRODUCTION

Ray methods, especially those designed to calculate synthetic wavefields, require velocity models composed of several smooth blocks separated by interfaces covered by smooth surfaces. The smaller the number of blocks and surfaces, the better. Such velocity models miss possible fine layering in the vicinities of the source and receivers or along structural interfaces. Since the frequency–dependent response of the stacks of fine layers may influence synthetic wavefields considerably, the ray–theory synthetic seismograms are too distorted if the stacks of fine layers are neglected.

This drawback of the ray methods can be corrected approximately if the "thin" stacks of fine layers are locally approximated by the 1–D stacks, the wave is locally approximated by a plane wave in each fine layer, and the matrix method is used to calculate the local response of each stack. The ray–theory elementary Green functions are then combined with the frequency–dependent matrix–method responses. For more details refer, e.g., to the papers by *Červený (1994)* and *Jílek and Červený (1994; 1995; 1996a,b)*.

Thomson (1998a,b) developed program package RMATRIX for the calculation of the frequency–dependent responses of the stacks of fine isotropic or anisotropic layers. The program package was included on the compact disk by *Klimeš (1998b)*. For the latest version of the software and data refer to *Bucha and Bulant (2017)*.

A simple 1–D velocity model, named RM, has been designed to debug the ray–matrix software and to compare the ray–matrix synthetic seismograms with the finite–difference synthetic seismograms. The corresponding test calculations together with the detailed specification of input data were described step–by–step by *Klimeš (1998a)*. In this paper, we concisely explain the method and present the main results of the test calculations.

2. METHOD

The receivers are assumed to be distributed in the vicinity of the reference surface. The traced rays terminate at the reference surface. The two–point rays from the point or finite source to the projections of the receivers onto the reference surface are calculated according to *Bulant (1996; 1999)*.

The thin stack of fine isotropic or anisotropic layers is assumed to be situated in the vicinity of the reference surface. Travel time at the projection of a receiver onto the bottom of the thin stack of fine layers is then calculated by the linear Taylor expansion using the travel time and slowness vector at the reference surface. The complex–valued vectorial amplitude is kept constant since the distance of the bottom of the thin stack of fine layers from the reference surface is assumed to be small.

The thin stack of fine isotropic or anisotropic layers is locally approximated by a 1–D stack of parallel layers. The wave is locally approximated by the plane wave and the matrix method is used to calculate the local response of each stack for each frequency at the receiver. The ray–theory elementary Green functions are then combined with the frequency–dependent matrix–method responses. For more details refer, e.g., to the papers by *Červený (1994)* and *Jílek and Červený (1994; 1995; 1996a,b)*.

3. APPROXIMATION OF A POINT SOURCE BY A LINE SOURCE IN A 2–D VELOCITY MODEL

Geological structures and their velocity models are generally 3–D, and the waves propagate in 3–D. Unfortunately, we may sometimes have a computer code for 2–D only. For example, we have a 2–D finite–difference code for comparison with the 3–D ray–matrix code in this study. We thus need to approximate the wavefield generated by a point source in terms of the wavefield generated by a line source in a 2–D velocity model.

The zero–order ray–theory approximation of the 3–D frequency–domain tensorial Green function from point $\mathbf{x}'$ to point $\mathbf{x}$ reads (*Klimeš, 2012, Eq. 55*)

$$G_{im}(\mathbf{x},\mathbf{x}',\omega) \simeq \frac{1}{4\pi}\,\frac{g_i(\mathbf{x})\,g_m(\mathbf{x}')}{\sqrt{\varrho(\mathbf{x})\,v(\mathbf{x})\,\varrho(\mathbf{x}')\,v(\mathbf{x}')}\,L(\mathbf{x},\mathbf{x}')}\,\exp[\mathrm{i}\,\varphi(\mathbf{x},\mathbf{x}')]\,\exp[\mathrm{i}\omega\,\tau(\mathbf{x},\mathbf{x}')]\quad . \tag{1}$$

Here ω is the circular frequency, g_i is the polarization vector, ϱ is the density, τ is the travel time, v is the corresponding phase velocity, φ is the phase shift due to caustics, and L is the relative geometrical spreading (*Červený, 2001, Eq. 4.14.45*; *Klimeš, 2012, Eq. 13*). In a 2–D velocity model, the relative geometrical spreading can be decomposed into the product of 2–D relative geometrical spreading $L^{\parallel}$ in the plane of symmetry and relative geometrical spreading $L^{\perp}$ perpendicular to the plane of symmetry (*Červený, 2001, Eq. 4.13.52*),

$$L(\mathbf{x},\mathbf{x}') = L^{\parallel}(\mathbf{x},\mathbf{x}')\, L^{\perp}(\mathbf{x},\mathbf{x}') \quad . \tag{2}$$

In an isotropic medium, relative geometrical spreading $L^{\perp}$ perpendicular to the plane of symmetry reads (*Červený, 2001, Eq. 4.13.54*)

$$L^{\perp}(\mathbf{x},\mathbf{x}') = \sqrt{\int_{\mathbf{x}'}^{\mathbf{x}} v\,\mathrm{d}s} \quad , \tag{3}$$

where propagation velocity v is integrated with respect to arclength s along the ray.

The zero–order ray–theory approximation of the 2–D frequency–domain tensorial Green function from the line source at point $\mathbf{x}'$ to point $\mathbf{x}$ reads (*Červený, 2001, Eqs 5.2.127–5.2.128*)

$$G^{\mathrm{2D}}_{im}(\mathbf{x},\mathbf{x}',\omega) \simeq \frac{\sqrt{2\pi}}{\sqrt{|\omega|}\exp[-\mathrm{i}\frac{\pi}{4}\mathrm{sgn}(\omega)]} \times \frac{1}{4\pi}\,\frac{g_i(\mathbf{x})\, g_m(\mathbf{x}')}{\sqrt{\varrho(\mathbf{x})\, v(\mathbf{x})\, \varrho(\mathbf{x}')\, v(\mathbf{x}')}\, L^{\parallel}(\mathbf{x},\mathbf{x}')}\, \exp[\mathrm{i}\,\varphi(\mathbf{x},\mathbf{x}')]\, \exp[\mathrm{i}\omega\,\tau(\mathbf{x},\mathbf{x}')] \quad . \tag{4}$$

Assume that we have wavefield $u_i^{\mathrm{2D}}(\mathbf{x},\omega)$ calculated by 2–D finite differences for a line source. Comparing relations (1) and (4), we see that we may approximate the 3–D wavefield corresponding to a point source by

$$u_i(\mathbf{x},\omega) = \sqrt{|\omega|}\, \exp\big[-\mathrm{i}\tfrac{\pi}{4}\mathrm{sgn}(\omega)\big]\, \sqrt{\frac{1}{2\pi\, L^{\perp}(\mathbf{x},\mathbf{x}')}}\, u_i^{\mathrm{2D}}(\mathbf{x},\omega) \quad . \tag{5}$$

The first two factors on the right–hand side represent the frequency filter corresponding to the halfth derivative of the line–source time function, and the third factor represents the amplitude scaling from a line source to a point source.

If we have a 2–D wavefield in a 2–D velocity model, transformation (5) may generally be very useful for practical applications in order to obtain the corresponding 3–D wavefield, provided that we can approximately decompose the complete wavefield into individual elementary waves which differ by relative geometrical spreading $L^{\perp}$ perpendicular to the plane of symmetry.

4. NUMERICAL EXAMPLE

A very simple 1–D velocity model consists of a low velocity layer covering a homogeneous halfspace. Vertical axis x_3 points downwards, the free Earth surface is situated at the depth of $x_3 = 0.000\,\mathrm{km}$. The thickness of the low velocity layer is $0.010\,\mathrm{km}$, with material properties $v_\mathrm{P} = 1.0\,\mathrm{km\,s^{-1}}$, $v_\mathrm{S} = 0.5\,\mathrm{km\,s^{-1}}$, $\rho = 1.6\,\mathrm{kg\,dm^{-1}}$. The velocities in real shallow sediments might be smaller but would imply a denser grid for finite differences. The homogeneous halfspace has material properties $v_\mathrm{P} = 3.2\,\mathrm{km\,s^{-1}}$, $v_\mathrm{S} = 2.0\,\mathrm{km\,s^{-1}}$, $\rho = 2.5\,\mathrm{kg\,dm^{-1}}$.

The point explosive source is located at depth $x_3 = 0.200\,\mathrm{km}$, below the origin of the Cartesian coordinates. The profile of 19 receivers spaced at $0.020\,\mathrm{km}$ along the Earth surface is centred above the source, see Fig. 1.

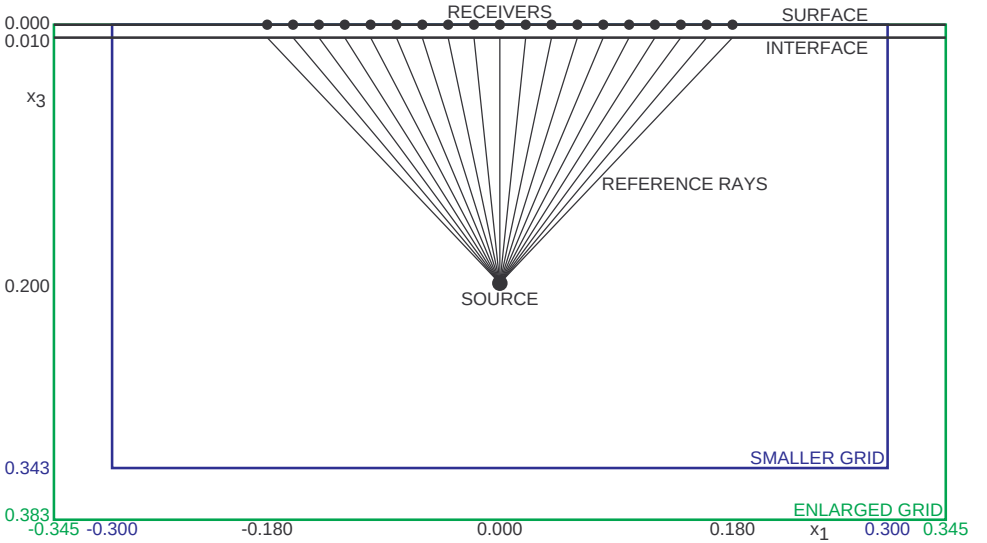

Fig. 1. Velocity model, source–receiver configuration, reference rays, smaller and enlarged grids for finite differences.

The sedimentary layer represents the fine local layered structures at the receiver locations and normally would not be contained within the macro velocity model. Here we need the sedimentary layer in the velocity model for the finite differences and use the same velocity model also for ray tracing. The two–point rays are thus caught at the top of the homogeneous halfspace, exactly below the receivers. In the ray–matrix method, the plane–wave approximation is used to extrapolate the wavefield from the endpoint of the two–point ray to the bottom of the thin local layer stack of fine layers and from the top of the layer stack to the receiver point.

We selected the Küpper signal (*Küpper, 1958*; *Müller, 1970*) with 2 local maxima for 2–D finite differences. The reference frequency of 20 Hz corresponds to the P–wave wavelength of 0.050 km in the sedimentary layer, i.e. 5 times the thickness of the layer.

We calculated the 3–D synthetic seismograms from the point explosive source using the 3–D ray–matrix method described in Section 2. However, we use 2–D finite differences for comparison, because we have no 3–D finite–difference code. The finite–difference seismograms thus correspond to a line source. We have used the line source excited by the Küpper signal at 3×3 gridpoints in the 2–D finite–difference program. For the point source in 3–D, we thus take the halfth derivative of the Küpper signal as the source time function describing the time dependence of the seismic moment of the explosive point source. Then the point and line sources generate wavelets of the same form in the far–field approximation. Note that the halfth derivative is defined by the frequency filter appearing on the right–hand side of transformation relation (5). Refer to Fig. 2 for the resulting point–source time function.

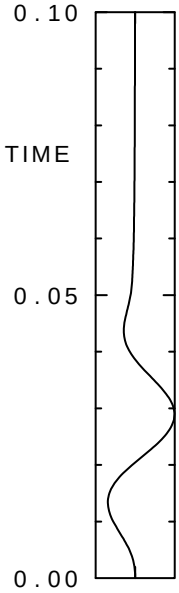

Fig. 2. Point–source time function.

In a homogeneous isotropic medium, relative geometrical spreading (3) perpendicular to the plane of symmetry reads

$$L^{\perp}(\mathbf{x}, \mathbf{x}') = \sqrt{v\, r} \quad , \tag{6}$$

where v is the propagation velocity and r is the hypocentral distance. To be able to plot 3–D ray–matrix seismograms corresponding to the point source and the 2–D finite–difference seismograms corresponding to the line source in a comparable scale, we choose the reference distance for the amplitude power scaling during the plotting equal to the hypocentral distance

$$R = (2\,\pi\, v_{\mathrm{P}})^{-1} \tag{7}$$

(in a homogeneous medium), at which the wavefields generated by the point and line sources have the same amplitudes, see transform (5). In plotting, we shall use no amplitude power scaling for the point source but the power scaling, proportional to the hypocentral distance powered to $-\frac{1}{2}$, for the line source. In this way, seismograms corresponding to the point and line sources will coincide in the neighbourhood of the source point. They, of course, might differ considerably at large distances in a heterogeneous medium.

Finite differences are often limited by the memory requirements or by the computational costs. This is also the case of the following grid dimensions. We covered horizontal axis x_1 from $-0.300\,\mathrm{km}$ to $0.300\,\mathrm{km}$ by $N_1 = 601$ gridpoints with grid intervals of $D_1 = 0.001\,\mathrm{km}$. We covered vertical axis x_3 from the depth of $0.000\,\mathrm{km}$ to the depth of $0.343\,\mathrm{km}$ by $N_3 = 344$ gridpoints with grid intervals of $D_3 = 0.001\,\mathrm{km}$. The finite–difference seismograms were calculated for 1601 time levels with the time step of $0.000175\,\mathrm{s}$.

P–wave travel time along the ray reflected from the bottom of the computational box and arriving at the middle receiver is

$$\tau_0 = \frac{2(N_3 - 11) * D_3 - 0.190\,\mathrm{km}}{3.2\,\mathrm{km\,s^{-1}}} + \frac{0.010\,\mathrm{km}}{1.0\,\mathrm{km\,s^{-1}}} \quad .$$

For $D_3 = 0.001\,\mathrm{km}$ and $N_3 = 344$, $\tau_0 = 0.15875\,\mathrm{s}$.

P–wave travel time along the ray reflected from the side of the computational box and arriving at the outside receiver ($x_1 = \pm 0.180\,\mathrm{km}$) is

$$\tau_1 \approx \frac{\sqrt{[(N_1 - 1) * D_1 - 0.180\,\mathrm{km}]^2 + [0.190\,\mathrm{km}]^2}}{3.2\,\mathrm{km\,s^{-1}}} + \frac{0.010\,\mathrm{km}}{1.0\,\mathrm{km\,s^{-1}}} \quad .$$

For $D_1 = 0.001\,\mathrm{km}$ and $N_1 = 601$, $\tau_1 \approx 0.154\,\mathrm{s}$.

Since the "non–reflecting" boundary conditions of finite differences may, to some extent, reflect the waves, it is highly recommended to change the finite–difference grid roughly by a quarter of the prevailing wavelength and to run the finite differences once again. The reflections from the boundaries are then shifted roughly by half the prevailing period and are clearly visible in the common plots of the seismograms from both the computations. The reference P–wave wavelength in the homogeneous halfspace is 160 grid intervals. We thus enlarge the grid by 40 grid intervals at the bottom and by 45 grid intervals at each side (increase of 40 to 45 accounts for the angle of reflection from the non–reflecting boundary, but 40 would be fine).

The calculated seismograms are shown in Figures 3 and 4, where the reflections from the non–reflecting boundaries (the bottom and sides of the finite–difference grid) can clearly be identified. The blue reflections (the first finite–difference calculation) come before the green ones (the second finite–difference calculation, with the enlarged grid).

The agreement between the ray–matrix (red) and finite–difference seismograms is very good except for a small difference at the horizontal component around time $t = 0.15\,\mathrm{s}$. The ray–matrix seismograms do not suffer from the reflections from the non–reflecting boundaries.

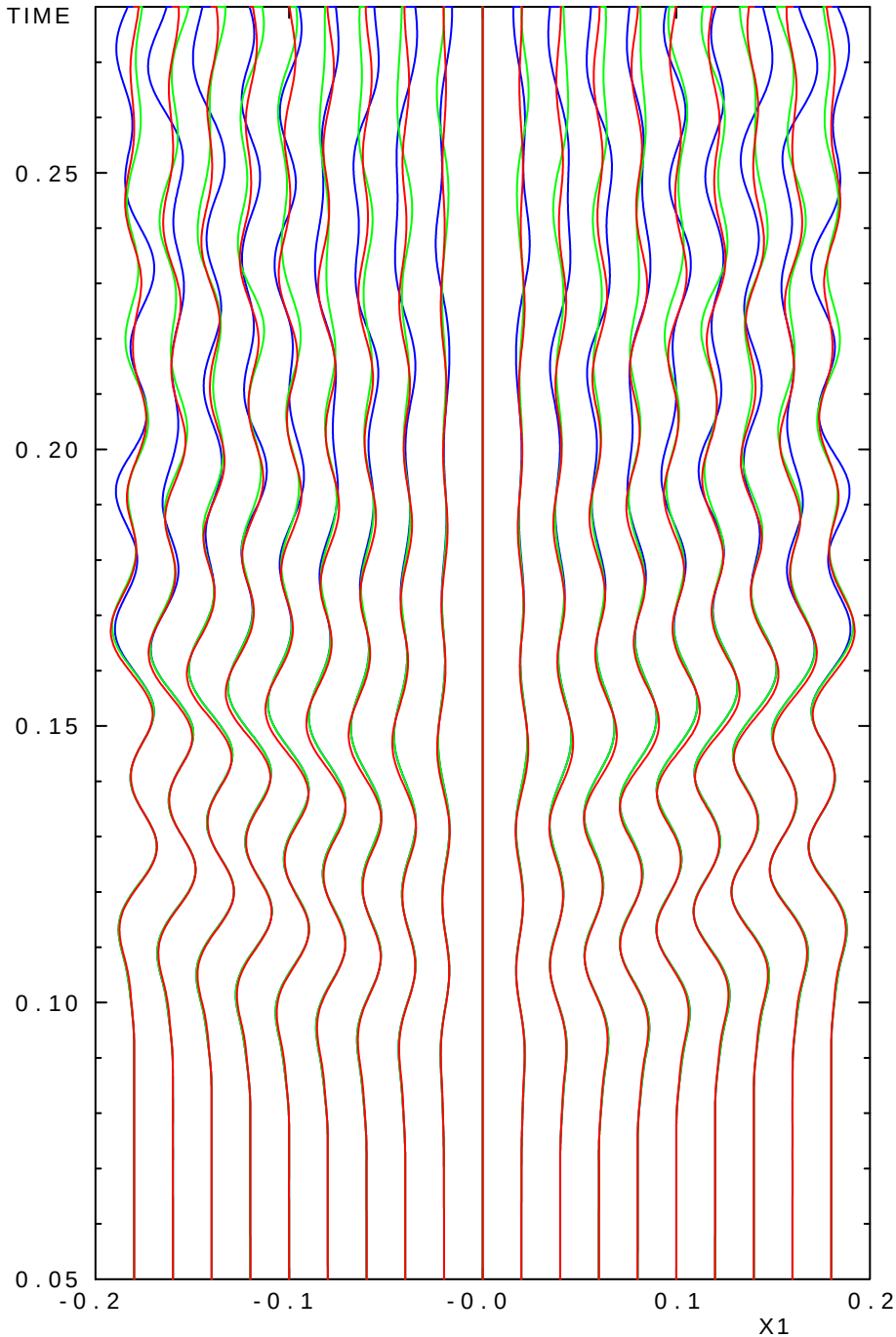

Fig. 3. Horizontal component. The 2–D finite differences are **blue** and **green**, the 3–D ray–matrix method is **red**.

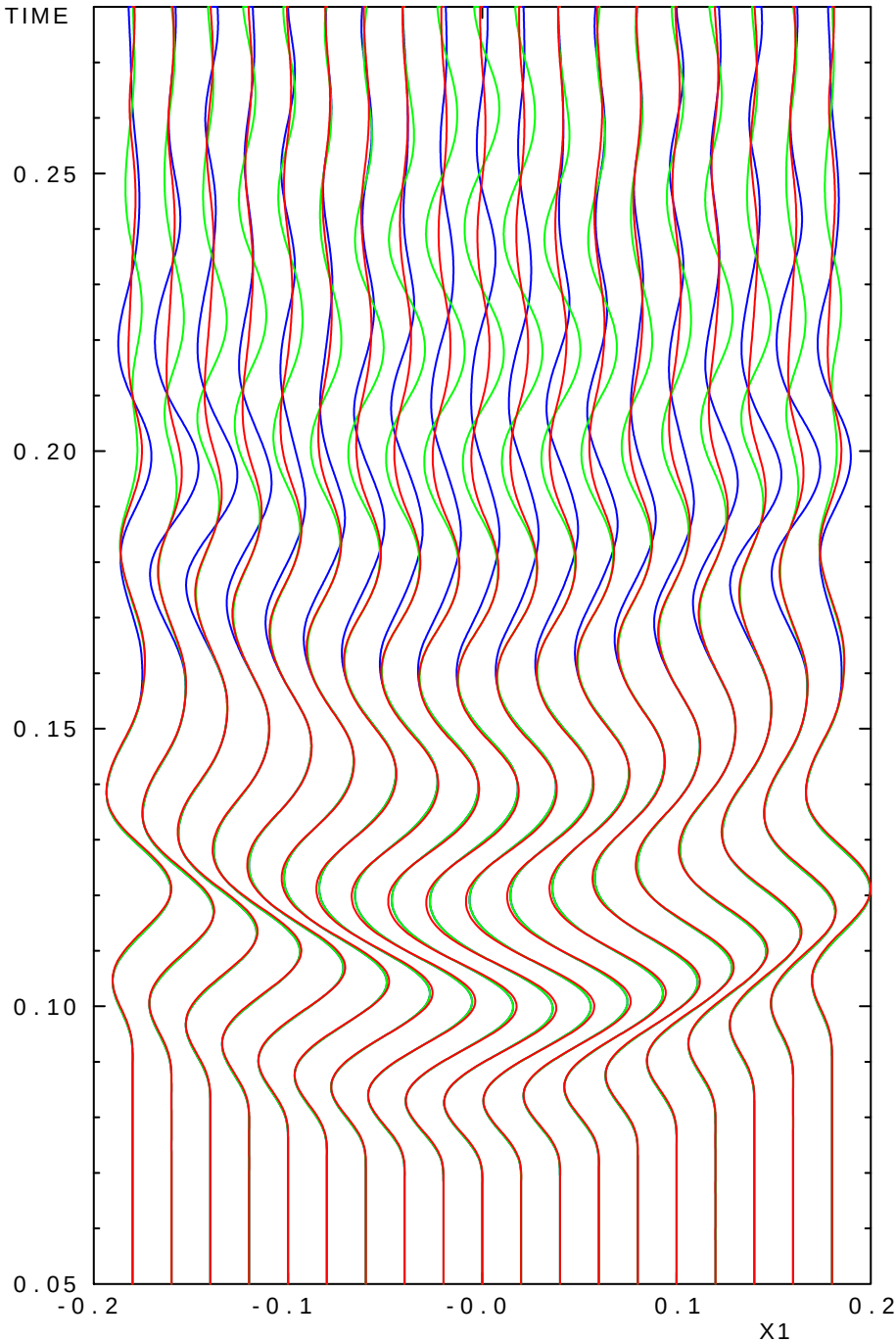

Fig. 4. Vertical component. The 2–D finite differences are **blue** and **green**, the 3–D ray–matrix method is **red**.

5. CONCLUSIONS

The ray–matrix method can extend the applicability of ray methods to 3–D heterogeneous velocity models containing thin stacks of fine isotropic or anisotropic layers. The good accuracy of this extension has been demonstrated in the numerical example.

Because of the comparison with an available finite–difference code, the ray–matrix method has been applied to a simple isotropic velocity model in this paper. However, the ray–matrix method is equally well applicable to heterogeneous generally anisotropic media.

Regardless of the ray–matrix method, transformation (5) may generally be very useful for practical applications if we have a 2–D wavefield in a 2–D velocity model and need to obtain the corresponding 3–D wavefield, provided that we can decompose the complete wavefield approximately into individual elementary waves which differ by the relative geometrical spreading perpendicular to the plane of symmetry.

Similarly, the method of identifying the reflections from the non–reflecting boundaries which we employed in the numerical example may be of a general interest in complete wavefield modelling methods.

Acknowledgements: The suggestions by an anonymous reviewer made it possible for me to improve the paper considerably. The research has been supported by the Grant Agency of the Czech Republic under contract 16-05237S, by the Ministry of Education, Youth and Sports of the Czech Republic within research project CzechGeo/EPOS LM2015079, and by the members of the consortium "Seismic Waves in Complex 3–D Structures" (see "http://sw3d.cz").

References

Bucha V. and Bulant P. (Eds), 2017. SW3D–CD–21 (DVD–ROM). *Seismic Waves in Complex 3–D Structures*, **27**, 133–134 (http://sw3d.cz).

Bulant P., 1996. Two–point ray tracing in 3–D. *Pure Appl. Geophys.*, **148**, 421–447.

Bulant P., 1999. Two–point ray–tracing and controlled initial–value ray–tracing in 3–D heterogeneous block structures. *J. Seism. Explor.*, **8**, 57–75.

Červený V., 1994. Influence of local structures close to the source and receiver on the seismic wave field. *Seismic Waves in Complex 3–D Structures*, **1**, 9–27 (http://sw3d.cz).

Červený V., 2001. *Seismic Ray Theory.* Cambridge Univ. Press, Cambridge, U.K.

Jílek P. and Červený V., 1994. Radiation patterns of point sources situated close to the Earth's surface. *Seismic Waves in Complex 3–D Structures*, **1**, 29–44 (http://sw3d.cz).

Jílek P. and Červený V., 1995. Radiation patterns of point sources situated close to structural interfaces and to the Earth's surface. *Seismic Waves in Complex 3–D Structures*, **3**, 175–228 (http://sw3d.cz).

Jílek P. and Červený V., 1996a. Radiation patterns of point sources situated close to structural interfaces and to the Earth's surface. *Pure Appl. Geophys.*, **148**, 175–225.

Jílek P. and Červený V., 1996b. Ray theory radiation patterns of point sources situated at structural interfaces. *Seismic Waves in Complex 3–D Structures*, **4**, 183–221 (http://sw3d.cz).

Klimeš L., 1998a. Comparison of ray–matrix and finite–difference methods in a simple 1–D model. *Seismic Waves in Complex 3–D Structures*, **7**, 169–180 (http://sw3d.cz).

Klimeš L. (Ed.), 1998b. SW3D–CD–2 (CD–ROM). *Seismic Waves in Complex 3–D Structures*, **7**, 405–405 (http://sw3d.cz).

Klimeš L., 2012. Zero–order ray–theory Green tensor in a heterogeneous anisotropic elastic medium. *Stud. Geophys. Geod.*, **56**, 373–382.

Küpper F.J., 1958. Theoretische Untersuchungen über die Mehrfachaufstellung von Geophonen. *Geophys. Prospect.*, **6**, 194–256 (in German).

Müller G., 1970. Exact ray theory and its application to the reflection of elastic waves from vertically inhomogeneous media. *Geophys. J. R. Astr. Soc.*, **21**, 261–284.

Thomson C.J., 1998a. Notes on waves in layered media to accompany program Rmatrix. *Seismic Waves in Complex 3–D Structures*, **7**, 147–162 (http://sw3d.cz).

Thomson C.J., 1998b. Notes on Rmatrix, a program to find the seismic plane–wave response of a stack of anisotropic layers. *Seismic Waves in Complex 3–D Structures*, **7**, 163–167 (http://sw3d.cz).